Scientific Reports

https://doi.org/10.1038/s41598-026-50144-7

Article in Press

Smart label-free SPR biosensing platform for hemoglobin and urine glucose detection via machine learning

Received: 26 February 2026

Accepted: 20 April 2026

Published online: 02 May 2026

Cite this article as: Reddy P.S.K., Chebaane S., Vasimalla Y. *et al.* Smart label-free SPR biosensing platform for hemoglobin and urine glucose detection via machine learning. *Sci Rep* (2026). https://doi.org/10.1038/s41598-026-50144-7

Parvathala Siva Kumar Reddy, Saleh Chebaane, Yesudasu Vasimalla, Sana Ben Khalifa, Norah A. M. Alsaif, Ravi Sankar Puppala, Bhishma Karki & Santosh Kumar

Smart Label-Free SPR Biosensing Platform for Hemoglobin and Urine Glucose Detection via Machine Learning

Parvathala Siva Kumar Reddy[1], Saleh Chebaane[2], Yesudasu Vasimalla[1],
Sana Ben Khalifa[3], Norah A.M. Alsaif [4] and Ravi Sankar Puppala[5], Bhishma karki[6,7,8]* ,Santosh Kumar[1]

[1]Centre of Excellence for Nanotechnology, Department of Electronics and Communication Engineering, Koneru Lakshmaiah Education Foundation, Vaddeswaram, Andhra Pradesh–522302, India, (Email: parvathalasiva57@gmail.com)

[2]Department of physics, College of Science, University of Ha'il, P.O.Box 2440, Ha'il , Saudi Arabia, (Email: chesaleh7@gmail.com)

[3]Department of Physics, College of Science, Qassim University, P.O.Box, 6644, Buraydah Almolaydah, 51452, Saudi Arabia, (Email: s.benkhalifa@qu.edu.sa)

[4]Department of Physics, College of Science, Princess Nourah Bint Abdulrahman University, P.O. Box 84428, Riyadh, 11671, Saudi Arabia, (Email: noaalsaif@pnu.edu.sa)

[5]Department of Computer Science Engineering, Amrita Viswa Vidya Peetham, Amaravati, India (Email: p_ravisankar@av.amrita.edu)
[5]Department of Computer Science Engineering, Amrita Viswa Vidya Peetham, Amaravati, India

[6]Department of Physics, Tri-Chandra Multiple Campus, Tribhuvan University, Kathmandu 44600, Nepal [7]National Research Council Nepal, New Baneshwor-10, Kathmandu 44600, Nepal

[8]Department of Physics and Research Centre, Tuljaram Chaturchand College, Baramati, Pune 413102, India

[1]Centre of Excellence for Nanotechnology, Department of Electronics and Communication Engineering, Koneru Lakshmaiah Education Foundation, Vaddeswaram, Andhra Pradesh–522302, India, (Email:santosh@kluniversity.in)

**Corresponding author's emails: Bhishma.karki@trc.tu.edu.np, magnum.photon@gmail.com;*

Abstract: This article presents the design and the numerical analysis of a smart label-free Surface Plasmon Resonance (SPR) sensor to detect the concentration of haemoglobin in blood and the concentration of glucose in the urine samples. The suggested sensor uses a thin film of silver (Ag) on the prism's surface to excite the surface plasmons. The finite element method (FEM) was used to do numerical simulations to optimize the layer thickness and to analyse the sensor's performance in terms of the sensitivity and the Figure of merit (FOM). The results of the simulation showed that there is a linear correlation between resonance wavelength shift and change in analyte refractive index. The optimised design obtained a sensitivity of 288.29 °/RIU, QF of 780.80 RIU^{-1}, SNR of 15.62, FoM of 492.51 RIU^{-1} and CSF of 539.20. The label-free methodology involves no chemical tagging and thus allows biosensing that is quick, real-time and economical. The suggested SPR sensor has great possibilities to be implemented in the non-invasive biomedical applications, diagnostics and point-of-care monitoring. In addition, machine learning models were employed to predict sensor sensitivity based on structural and optical parameters, demonstrating the strong capability of data-driven approaches for rapid performance estimation and design optimization.

Keywords: surface plasmon resonance, label-free biosensor, haemoglobin detection, glucose sensing, biomedical applications, machine learning.

1. Introduction

The rapid development of genetics and biochemistry has resulted in the development of a range of medical and biomedical tools to identify a variety of disorders with incredible precision. Optical-based sensing is currently leading biosensors because of the several properties of absorption, transmittance and reflectance of light waves to the variation in the medium around it [1]. The sensing of continuous glucose monitoring devices is also painful, but this is also used for sensing purposes [2, 3]. The alternative method to glucose detection is known as a fluorescent glucose biosensor. Among optical biosensing technologies, the surface plasmon resonance biosensor (SPRB) is particularly useful in medicine because of its remarkable features, including high sensitivity, direct and rapid detection, fast separation, spectral selectivity and large local electric field enhancement [4, 5].The SPRB works by the binding of the receptor molecule to the sample analyte, resulting in an alteration of the refractive index, which causes the refractive index of the bio-membrane layer to change, which subsequently generates a measurable response, like a shift of the resonance peak[[6]][[7]]. The proposed sensor design aims to provide an efficient, cost-effective, and portable diagnostic tool for early detection and management of diabetes mellitus. Surface Plasmon Resonance (SPR) has emerged as one of the most powerful optical sensing techniques for real-time and label-free detection of biomolecules. Unlike conventional biochemical assays that require fluorescent or enzymatic labelling, SPR enables direct monitoring of molecular interactions at the sensor surface through variations in the refractive index[7]. The technical strategies used in biosensors are based on label-based and label-free strategies of detection. Label-based detection is based on the distinctive characteristics of labelled compounds to use as a target. Even though these biosensors are reliable, they usually require a combination of specific-sensing elements and immobilised target protein[8]. The iron-carrying metalloprotein within the red blood cells, haemoglobin (HB) is made of four globin subunits, with each being attached to a heme group. Haemoglobin in its deoxy form (Fe2+) binds O2 to give oxyhaemoglobin, aiding oxygen delivery throughout the body[9]. The metalloprotein of the red blood cells, which is iron-bound, is called haemoglobin (HB) and consists of four globin subunits with each of which is bound to a heme group. Oxygen is bound to the deoxy form of haemoglobin (Fe2+) to form oxyhaemoglobin used in the body to transport oxygen [10]. The use of SPR-based biosensors is also promising due to the possibility of sensing even a slight change in concentrations of biomolecules, without involving fluorescent or radioactive labels. When the sensing layers are optimized well in terms of structure, such as using metallic films and dielectric substrates, SPR sensors can attain high sensitivity, specificity and reproducibility[11]. Biosensors based on SPR provide a special benefit over other strategies to overcome these difficulties because of their high sensitivity, quick reaction, potentially small size, and integration with microfluidic systems. Optimisation of sensor architecture, including selection of plasmonic materials, dielectric over-layers and prism coupling configurations, are numerically modelled to enhance the performance parameters, including sensitivity, Full-width half maximum (FWHM), detection accuracy, and figure of merit (FOM)[12].This sensor is especially favourable for real-time monitoring of environmental applications with respect to sensitivity, selectivity and operational simplicity compared to other methods. SPR sensors are a chance to conduct early and non-invasive diagnostic procedures. It is possible to create quantitative and stable detection protocols through the study of the refractive index changes with changes in physiological concentrations of haemoglobin in the blood plasma and glucose in the urine samples. Furthermore, numerical optimization by any means, including Transfer Matrix Method (TMM), Finite Difference Time Domain (FDTD) or simulation via MATLAB enables a sensor geometry to be optimized accurately before physical implementation[13]. This paper reports the discovery of surface plasmon resonance (SPR) sensor based on BK7 prism is used in combination with a silver (Ag) thin film to increase plasmon excitation and more dielectric and nanocomposite layers are also added to increase the sensitivity and reduce optical losses. Recent studies have demonstrated that machine-learning (ML) techniques can significantly enhance the analysis and optimisation of SPR-based biosensors by learning complex nonlinear relationships between structural parameters and sensing performance [14, 15].

Regression and neural network-based models have been successfully applied to predict resonance wavelength shifts, sensitivity, and figure of merit directly from multilayer thicknesses and refractive index variations [16, 17]. Tree-based ensemble methods such as Random Forest and boosting algorithms have also shown high predictive accuracy and strong feature-selection capability in plasmonic sensing systems[18]. The integration of ML with numerical simulation enables rapid virtual prototyping, reduces computational cost, and provides deeper physical insight into parameter influence for biosensing applications [19, 20]

2. Design and Methodology

Surface Plasmon Resonance (SPR) is one of the label-free detection techniques used in research, especially in the examination of biomolecular interactions such as haemoglobin. The environmental harmlessness and relevance to clinical research are put into the spotlight of SPR. This step produces the design and methodology label-free surface plasmon resonance (SPR) sensor in Kretschmann configuration with a BK7 prism, a thin layer of titanium as an adhesion layer, and gold sensing film with the highest sensitivity. The system was irradiated at 633 nm wavelength using a HeNe laser, and resonance angle displacement was observed to identify changes in refractive index by the haemoglobin and glucose molecules. Blood, urine samples were filtered and applied to the sensing surface under controlled temperature in phosphate-buffered saline, with blood samples being anticoagulated and diluted.

2.1 Design considerations

As shown in Fig. 1, the proposed surface plasmon resonance (SPR) sensor is constructed in a Kretschmann configuration that incorporates a BK7 prism, Ag layer and thin titanium adhesion layer to achieve high sensitivities to haemoglobin in blood and glucose in urine. Mixed self-assembled monolayers of haemoglobin-specific receptors on the gold surface and glucose-binding phenylboronic acid derivatives are functionalized to selectively pull down the analyte[21, 22]. phase velocity and mode coupling are governed by the real quantity of the refractive index, and absorption and dissipative loss in the material are governed by the imaginary quantity (the extinction coefficient, k)[23]. In the case of the metals and semiconducting/phase-change layers in this case, the complex refractive indices are employed to appropriately model the surface plasmon polariton (SPP) excitation and propagation losses[24, 25]. The multilayer SPR structure designed has a BK7 glass substrate is 1.515, a silver (Ag) plasmonic layer with optimised thickness, and functional overlayers of Hafnium dioxide (HfO_2) is having of 1.8943, Vanadium dioxide (VO_2) is having of 3.0459 + 0.3278i, and Aluminium antimonide (AlSb) is having of 3.8638 + 0.0036i, and then the optical confinement, tunability and stability of each layer were balanced[26, 27]. The thickness of the Ag layer was optimised (30 - 60 nm) to have a maximal surface plasmon resonance (SPR) sensitivity and minimum loss[28]. The thin layer of (HFO_2) enhances adhesion and protective properties on the metal, whereas VO_2 and AlSb adds active and interfacial tuning properties[29, 30]. The entire structure allows high field confinement and shifts in the resonances, which can be measured in the range of the analyte refractive index, which is characteristic of aqueous biological samples[31]. Finally, the sensing medium (SM), which have the presence of target analyte. From the literature, we found that the RI of 1.32919, 1.33019, 1.33519 1.34019, 1.34519, 1.34919 for HB in blood concentration of 6.1025 g/l, 36.615 g/l, 67.1275 g/l, 97.640 g/l, and 122.05 g/l, respectively. The RI of 1.35, 1.336, 1.337, 1.338, 1.341 and 1.347 for the urine glucose concentrations of 0 - 15 mg/dl, 0.625 gm/dl, 1.25 gm/dl, 2.5 gm/dl, 5 gm/dl and 10 gm/dl, respectively [32].

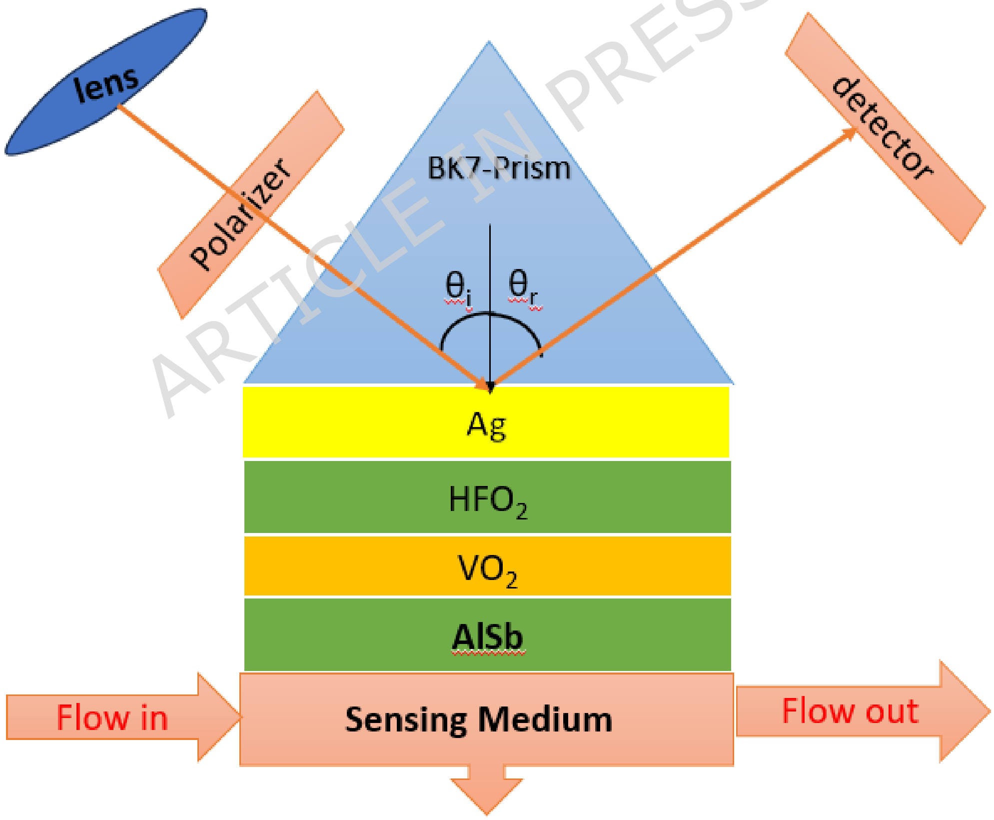

Fig 1. Schematic structure of the proposed sensor.

2.2 Methodology

The use of the Kretschmann configuration, which involves a high-refractive index BK7 prism, a thin silver (Ag) coating and the sensing media (blood or urine sample) is the proposed label-free SPR sensor. The prism directs a p-polarised beam of HeNe laser (λ = 633 nm) to emanate the surface plasmons at the interface between the metal and the sample [33]. Where, k_x represents parallel component of the incident wave vector and k_{spw} represents surface plasmon wave vector. The Transfer Matrix Method (TMM) was used to model the multilayer structure of the SPR sensor. In this, the incident and transmitted fields of electromagnetism are associated with the successive layers of dielectric and metallic layers. The transfer matrix of the multilayer stack is, in general, the following:

The surface plasmon wave vector is expressed in Eq. (1):

$$|kx = |kspw| \tag{1}$$

The SPR resonance angle is given in Eq. (2) [34].

$$\theta_{SPR} = \left(\sin^{-1} \sqrt{\frac{r_m^2 r_d^2}{r_p^2 \left(r_m^2 + r_d^2\right)}} \right) \tag{2}$$

where r_P, r_m and r_d are refractive index (RI) for the prism, metal film and dielectric layer, respectively. The reflection intensity for p-polarized light is expressed as [33]: Reflectivity (F_p) and its corresponding coefficient (f_p) are expressed in Eqs. (3) and (4), respectively, that are useful for investigating the optical response of sensors. Likewise, Equations (5) to (9) explore the various terms used in the equations. (4) and (5), respectively. The transvers RI of the x^{th} layer, presented by b_x, is given by Eq. (6). Additionally, the "characteristic matrix of the integrated sensor structure (V_{if})" for P-polarized incident light was described in Eq. (7), whose plays a major role in determining the interaction of light with the multilayer system. The reflection intensity for p-polarized light is expressed as: Furthermore, Eq. (7) which defined as β_x, is the free arbitrary phase constant of the x^{th} layer. Equations (9) and (10) provide values for the input angle (θ_x) and wave impedance (s_x) features at the x^{th} layer, respectively. In addition to it, permittivity (ε_x), permeability (μ_x), and thickness (d_x) of the layer are important parameters, which defines its optical and electromagnetic properties, thereby influencing the behaviour of wave transmission and reflection in the multilayer sensor.

$$F_p = f_p f_p^* = |f_p|^2 \tag{3}$$

$$f_p \frac{(F_{11} + F_{12} b_x) b_1 - (F_{21} + F_{22} b_x)}{(F_{11} + F_{12} b_x) b_1 + (F_{21} + F_{22} b_x)} \tag{4}$$

$$b_N = \frac{\varepsilon_x}{\mu_x}\cos\theta_x, \text{ where } \quad \cos\theta_x = \sqrt{\frac{\varepsilon_x - (r_p \sin\theta)^2}{\varepsilon_x^2}} \tag{5}$$

The Transfer Matrix Method (TMM) was used to model the multilayer structure of the SPR sensor. In this, the incident and transmitted fields of electromagnetism are associated with the successive layers of dielectric and metallic layers. The transfer matrix of the multilayer stack is in general the following [33]:

$$F_{if} = \left[\prod_{x=2}^{N-1}\begin{pmatrix}\cos\beta_x & \frac{i}{b_x}\sin\beta_x \\ ib_x \sin\beta_x & \cos\beta_x\end{pmatrix}\right]_{if} = \begin{bmatrix}F_{11} & F_{12} \\ F_{21} & F_{22}\end{bmatrix} \tag{6}$$

$$\beta_x = \frac{2\pi}{\lambda} n_x d_x \cos\theta_x$$

$$\theta_x = \sin^{-1}\left(\frac{n_p}{n_x}\sin\theta_{inc}\right)$$

$$b_x = \frac{n_x \cos\theta_x}{(\eta_0)} \tag{9}$$

$$F_{123456} = |f_{12.....n}|^2 = \left|\frac{f_{12} + f_{2....n}\, e^{2iw_2 d_2}}{1 + f_{12}\, f_{2....n}\, e^{2iw_2 d_2}}\right|^2 \tag{10}$$

Since Hemoglobin concentration in blood and glucose levels in urine alter the refractive index of the sample, the designed SPR sensor can be used as a label-free biosensing platform for their detection. The mathematical expressions, which are used to analyse the sensor's performance, are taken from literature [33, 34].

3. Results and Discussion

In this design, we present the simulation results of numerical modelling of the proposed label-free surface plasmon resonance (SPR) sensor revealed a sharp resonance dip at 633 nm, which was centrally shifted in response to target analyte concentration. To optimize the layers' thickness, we consider the better performance of minimum reflectance (R_{min}) and sensitivity. R_{min} demonstrates the maximum incident light's energy absorbs by the sensor, whereas the sensitivity states the sensing capacity of the sensor [34].

3.1 Optimizing Ag's thickness to enhance the sensor performance

This subsection shows the optimization of Ag thickness using the iteration method. Fig. 2 shows the reflectance curves with respect to the incident angle for the considered Ag thicknesses, where Fig. 2(a) and Fig. 2(b) for the sensing medium’s RI of 1.32919 and 1.34919, respectively. It is observed that the reflectance-angle stacks in the (Ag thickness varied ≈48–56 nm) show that the SPR dip depth and sharpness depend strongly on Ag thickness. Thin films (<54 nm) produce shallower, broader resonances (lower contrast and larger FWHM), while very thick films (>54 nm) begin to reduce coupling efficiency and slightly broaden the resonance again. The curves shows that FWHM increases with respect to the Ag thickness due to the damping effect, whereas SPR dip changes confirm the SPR property.

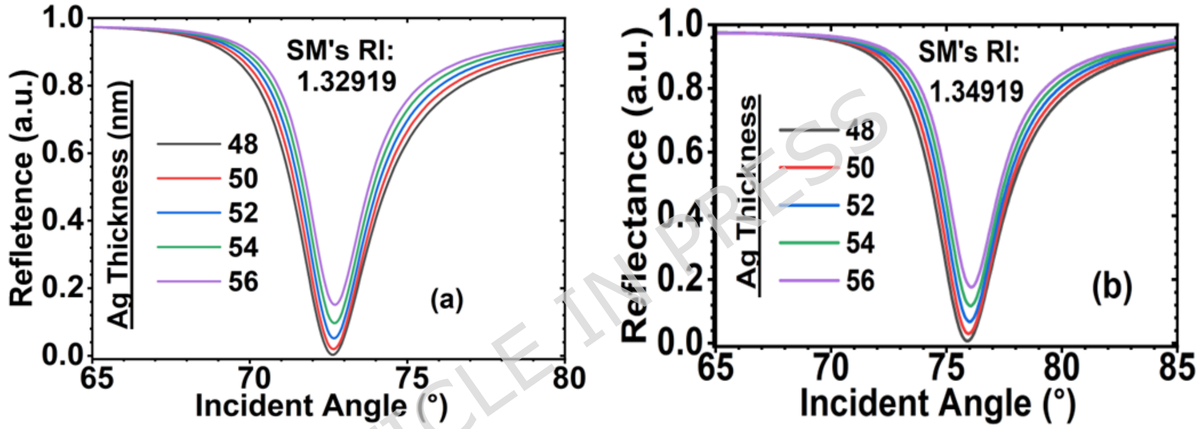

Fig. 2 Reflectance curves with respect to the angle for different Ag thicknesses at (a) SM’s RI of 1.32, and (b) SM’s RI of 1.34.

Table 1 indicates the parameters together with the Resonant angle, minimal reflectance(R_{min}), maximum reflectance,(R_{max}),FWHM, sensitivity, Quality factor(QF), signal-to-noise ratio(SNR), Figure of merit(FOM). The simulation results reveal that the lower ag thickness (40-45nm) produced broader resonance of curves with higher (R_{min}), indicating weak confinement of surface plasmon resonance. As the thickness increased, the resonance curves became sharper sensitivity and selectivity improved. The peak performance was recorded at the Ag thickness of 54 nm with the resonance angle between 72.6637° at RI of 1.32919 to 76.0591°/RIU at RI of 1.34919 with a sensitivity of 169.77 °/RIU. Therefore, the optimised value ag thickness is (54 nm) and was chosen to be used in further design with the best balance of reflectance, high sensitivity and sharp resonance.

Table 1: The measured parameters using Prism/Ag/HfO_2/VO_2/Analyte

Parameters	SM's RI	Ag thickness (nm)				
		48	**50**	**52**	**54**	**56**
θ_{res}(°)	1.32919	72.5996	72.6637	72.6637	72.6637	72.7277
	1.34919	75.9309	75.9309	75.995	76.0591	76.0591
R_{max}	1.32919	0.99191	0.98746	0.99259	0.9886	0.9932
	1.34919	0.98966	0.99374	0.99064	0.99423	0.99152
R_{min}	1.32919	0.0030268	0.0071898	0.019643	0.030162	0.051447
	1.34919	0.06758	0.096327	0.11737	0.15108	0.17592
FWHM (°)	1.34919	2.9875	3.5241	2.7339	3.2351	2.4759
	1.32919	2.9347	2.2163	2.6254	2.9557	2.3095
$\nabla\theta_{res}$ (°)		3.3313	3.2672	3.3313	3.3954	3.3314
Sensitivity (°/RIU)		166.565	163.36	166.565	169.77	166.57
QF (RIU^{-1})		55.7539	47.2063	60.9257	52.4775	67.2765
SNR		1.1150	0.9271	1.2185	1.0495	1.3455
FoM		0.8231	0.6480	0.2041	0.594	2.467
CSF		0.9891	0.9873	0.9924	0.9882	0.9928

3.2 Proposed structure impact

After optimizing the Ag thickness, this subsection shows the impact of the proposed structure, where its performance is compared with other considered structures that are made-up with the defined layers. Fig. 3 depicts the reflectance intensity curves corresponds to the incident angle for the different considered structures, S1-S5, whereas Fig. 3(a) and Fig. 3(b) represent for SM's RI of 1.32 and 1.34, respectively. S1 (Prism/Ag/SM) has a wider resonance with more distinct resonance minimum reflectance, and the addition of intermediate dielectric layers (AlSb, HfO_2, VO_2) in S2-S5 increases the strength of the coupling progressively, which leads to deeper resonance dips and smaller linewidths. This shows that the multilayer stacks enhance confinement of the evanescent field and hence enhance sensor performance. Table 2 quantitatively compares the parameters that were measured in the five structures at analyte refractive indexes of 1.32919 and 1.34995. The resonance angle varied by 2.49° - 3.52° across the designs with sensitivities of 0.0083 °/RIU(S1) to 169.73 °/RIU (S5). Remarkably, S1 had low sensitivity, which proves that a bare Ag interface cannot be used in high-performance biosensing. In comparison, the use of a structure with HfO_2 and VO_2 dielectric spacers (S3, S4, and S5) substantially enhanced the sensitivity (>130°/RIU).

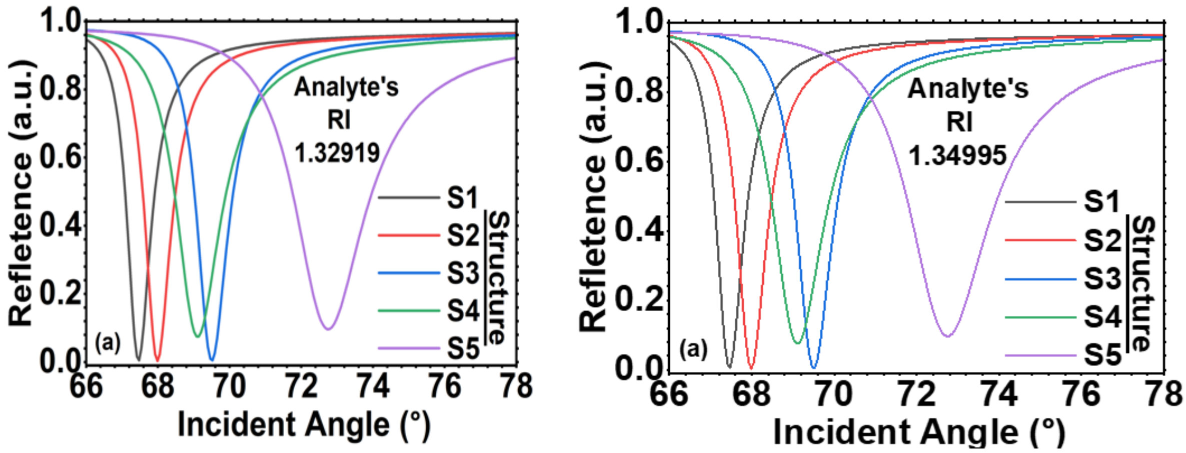

Fig. 3: Reflectance Curves with respect to SM's RI values for different considered structures at SM's RI of 1.32919 and (b) 1.34919.

Table 2: The measured parameters with respect to angle of SM's RI values of 1.32 & 1.34 for S1: Prism/Ag/SM, S2: Prism/Ag /Alsb /SM Prism, S3: Prism/Ag/HfO_2/SM, S4: Prism/Ag/VO_2/SM, S5: Prism/Ag/HfO_2/VO_2/Alsb/SM

Structure	R_{min}	FWHM (°)	Resonance angle (°)		$\nabla\theta_{res}$ (°)	Sensitivity (°/RIU)
			1.32919	1.34995		
S1	0.0052024	0.8320	67.4104	69.7808	2.3704	118.52
S2	0.003324	0.9160	67.9229	70.4214	2.4985	124.925
S3	0.0046591	1.0848	69.4605	72.0871	2.6266	131.33
S4	0.075065	1.4483	69.0761	71.7027	2.6266	131.33
S5	0.096327	2.2163	72.6637	76.0591	3.3954	169.77

Table 2 indicates the performance of five plasmonic structures (S1-S5) at the refractive indices of 1.32919 and 1.34995 of the analyte. There are observed clear structural design differences. The simple set-up (S1: Prism/Ag/SM) provided a minimal resonance shift (2.49°) and also showed low sensitivity (123.439°/RIU) in the resonance shifting. Even though it was the narrowest (FWHM = 0.96), its insignificant sensitivity proves that (S2: Ag/AlSb) and S3 (Ag/HfO_2) recorded sensitivities greater than 120°/RIU, with sharp resonance curves (FWHM = 1.06 - 1.27), which provides a good resolution/sensitivity balance. Subsequent improvements were made in S4 and S5 of VO2 multilayers; respectively, the sensitivity rose to 132.69°/RIU (S4) and 169.72°/RIU (S5). Nonetheless, S5 exhibited the largest linewidth (2.64), which decreased the resolution despite having the highest sensitivity.

3.3 **2D materials**

To assess the sensing performance of the optimised SPR device, we bonded the Ag film at 54nm and tested various combinations of 2D materials-AlSb, BP, graphene, MoS_2, $MoSe_2$, WS_2 and WSe_2. Figures 4 demonstrate the reflectance curves with respect to the incident angle at the analyte of 1.32919 and 1.34919 that shows in Fig. 4(a) and Fig. 4(b), respectively. Tables present the most important measured values: sensitivity, quality factor (QF), signal-to-noise ratio (SNR), figure of merit (FoM), and combined sensitive factor (CSF).

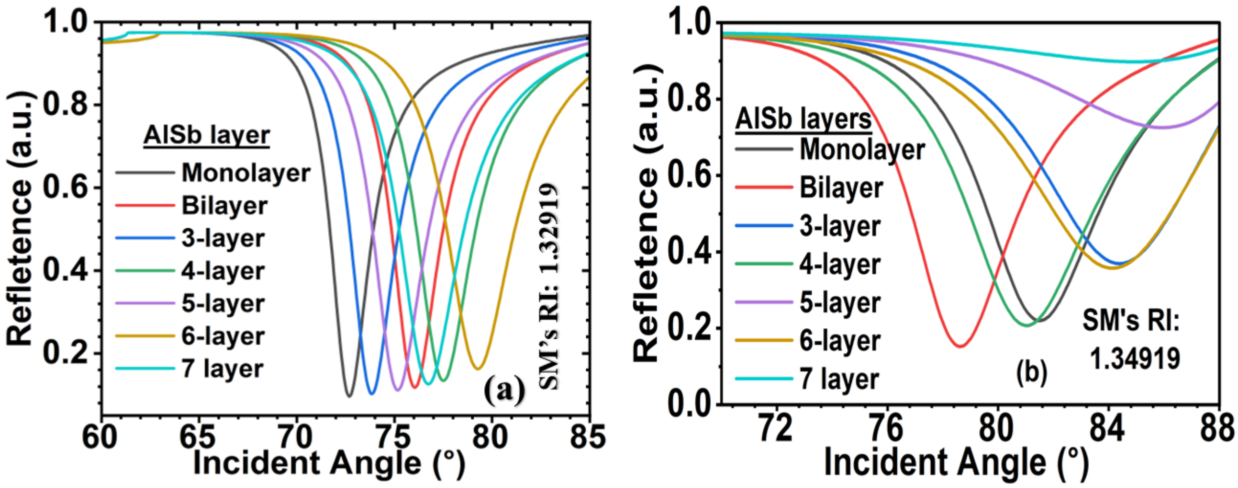

Fig.4 Reflectance Curves of AlSb with respect to angle of different AlSb layers at SM's RI of (a) 1.32919 and (b) 1.34919.

Table 3. The obtained parameters for Figure 4

AlSb layer	R_{min}	R_{max}	FWHM (°)	Resonance angle (°)		$\nabla\theta_{res}$ (°)	Sensitivity (°/RIU)
				1.32919	1.34919		
1	0.096327	0.9937	2.2163	72.6637	76.0591	3.3954	169.77
2	0.10207	0.9925	2.5101	73.8168	77.4685	3.6517	182.86
3	0.11099	0.9905	2.8613	75.1622	79.2623	4.1001	205.01
4	0.12601	0.9868	3.2808	76.6997	81.5045	4.8048	240.24
5	0.15224	0.9783	3.7622	78.6216	84.3874	5.7658	288.29
6	0.20728	0.9745	4.2901	81.0561	85.9248	4.8687	243.44
7	0.35732	0.9744	3.9124	84.1311	84.964	0.8329	41.65

Table 3 summarizes the experimentally determined values of parameters of the sensor configuration of Sensitivity, Quality Factor (QF), Signal-to-Noise Ratio (SNR), Figure of Merit (FoM), and Contrast Sensitivity Factor (CSF) of various numbers of AlSb (Aluminium Antimonide) layers added to the sensor structure. The findings indicate that there are significant differences in optical response and sensing behaviour with an increase in the number of AlSb layers between one and seven. The sensitivity values are not very high, between 0.00344°/RIU and 0.02945°/RIU , which means that AlSb is a stability contributor rather than the high refractive index responsiveness contributor. The QF reduces slowly at an average of 76.50797RIU^{-1} for one layer to 38.0783RIU^{-1} with six layers imply that the resonance sharpness reduces due to additional thickness. Some interesting variation is, however, noticed at seven layers, which is the maximum QF of 41.6585RIU^{-1}, probably because of the interference effect in the multilayer structure.

Table 4. Calculation of Sensitivity, QF, SNR, FoM and CSF for Graphene.

No. of Graphene layers	Sensitivity (°/RIU)	QF (RIU^{-1})	SNR	FoM (RIU^{-1})	CSF
1	163.554	74.2044	1.5404	74.0283	73.5459
2	166.42	70.8170	1.4721	70.5631	70.0249
3	169.730	71.0524	1.4750	70.7299	70.0904
4	175.895	77.1604	1.6018	76.7777	75.9598
5	184.099	95.4721	1.9820	78.3999	77.2055
6	195.098	97.4821	1.9921	79.3891	79.4593

Table 4 shows the derived values of sensitivity, QF, SNR, FoM and CSF when the number of Graphene layers was varied in the sensing structure. As the number of graphene layers rises, the sensitivity increases gradually, and the sensitivity to 163.5°/RIU becomes 195.098°/RIU which means that the more the number of layers of graphene it has, the more sensitive it is to detection. The SNR values increase to 1.9921 as compared to 1.5404, and this proves that the more layers that are added, the better the quality of the signal and its stability. On the same note, FoM and CSF have an upward trend with superior sensing performance and contrast sensitivity

Table 5. Calculation of Sensitivity, QF, SNR, FoM and CSF for MOS_2

No. of MoS_2 layers	Sensitivity (°/RIU)	QF (RIU^{-1})	SNR	FoM (RIU^{-1})	CSF
1	175.895	67.6727	1.4048	67.3581	66.6746
2	177.982	68.4756	1.4896	68.1610	67.4694

Table 5 reports the results of the computed parameters, namely sensitivity, QF, SNR, FoM and CSF of various numbers of MoS_2(Molybdenum Disulfide) layers included in the sensor structure. The findings indicate that the addition of one to two layers of MoS_2 does not significantly change the sensitivity which is 175.895°/RIU to 177.982°/RIU, but there is a slight increase in the capability of the sensor to record the changes in the refractive index. On the same note, the values of QF, FoM and CSF values are incremental but with small but steady increase, which is a better resonance sharpness and detection level with multi-layers MoS_2. The SNR increases to better value of 1.4896 implying a more stable and stronger output signal. There is also an increment in change in refractive index which changes 3.6516 to 3.8719 which validates the optical tunability of the layered MoS_2 structure.

Table 6. Calculation of Sensitivity, QF, SNR, FoM and CSF for WS_2

No. of WS_2 layers	Sensitivity (°/RIU)	QF (RIU^{-1})	SNR	FoM (RIU^{-1})	CSF
1	185.134	67.5770	1.4029	67.3978	62.1406
2	225.165	62.8794	2.7738	62.5934	61.3107

Table 6 results of the calculation of the optical performance parameters of sensitivity, QF, SNR, FoM and CSF are explained under varying numbers of WS_2 (Tungsten Disulfide) layers in the sensor configuration. The findings reveal that the level of sensitivity when the number of WS_2 layers is more than one, that is, two, increases by a substantial margin, that is, 185.134°/RIU to 225.165°/RIU, This demonstrates a significant increase in the ability of the sensor to detect. The net sum of all sensing performance is better despite the slight reduction of the QF and FoM between 67.5770, 62.8794, 67.3978 and 62.5934, respectively; the SNR gain is tremendously high and rises drastically between 1.4029 and 2.7738. This implies that multilayer WS_2 gives the signal a greater and more stable output.

Table 7. Calculation of Sensitivity, QF, SNR, FoM and CSF for WSe_2

No.of WSe_2 layers	Sensitivity (°/RIU)	QF (RIU^{-1})	SNR	FoM (RIU^{-1})	CSF
1	175.900	68.1254	1.4142	67.9398	67.3880
2	211.917	66.6238	1.3831	66.3397	65.3870
3	237.615	74.4431	1.5454	74.0463	72.1257

Table 7 shows the calculated optical sensing parameters, i.e. sensitivity, QF, SNR, FoM and CSF of increasing the number of WSe_2 (Tungsten Diselenide) layers incorporated in the sensor structure. The findings show that the sensitivity steadily rises as the number of layers of WSe_2

increases, which is 175.900 RIU^{-1}in the single layer and 237.615 RIU^{-1}in the triple layers, showing that the more the layers, the better the detection performance. Despite the fact that at first, the QF changes down to 68.1254RIU^{-1} and then comes to 66.6238RIU^{-1}, it increases to 74.4431 RIU^{-1} with three layers, implying that resonance sharpness increases with increasing layer thickness. The values of SNR are stable in the range of 1.38-1.54. The similarities between FoM and CSF are that they have similar increasing trends that confirm improved sensing precision and contrast sensitivity. The refractive index (DI) change is also enhanced when 3.6517 is changed to 4.9329, which shows that the optical response of multilayerWSe_2 films can be tuned.

Table 8. Calculation of Sensitivity, QF, SNR, FoM and CSF for $MoSe_2$.

No. of $MoSe_2$ layers	Sensitivity (°/RIU)	QF (RIU^{-1})	SNR	FoM	CSF	Change in RI
1.32919	175.900	67.7763	1.4070	67.4891	66.8520	3.6517
1.34995	200.587	68.0497	1.6042	67.6088	66.3839	4.1642

Table 8 shows the optical performance parameters of sensitivity, QF, SNR, FoM and CSF of the proposed sensor structure using $MoSe_2$ (Molybdenum Diselenide) of various thicknesses (or a small margin of 1.32919 to 1.34995, the ability to detect improves slightly by 175.900 RIU^{-1} to 200.587 RIU^{-1}, which proves that the more the material is interacted with, the better it tends to be detected. The QF is almost the same at approximately 68RIU^{-1}, which means that the resonance is sharp and does not change, and SNR increases 1.4070 to 1.6042, which displays the existence of better signal strength and stability. There are slight changes in the FoM and CSF, which have values of approximately 67.5 and 66 respectively indicating consistency in optical performance. The variation of the refractive index is 3.6517 to 4.1642 shows that the optical performance of the$MoSe_2$layer is tunable.

After comparing the performance of considered 2D materials, the proposed structure with AlSb layer offers better performance compared to others. Therefore, we use this structure to detection the HB in blood and urine detection. Fig. 5 depicts the reflectance curves with respect to the incidence angle for different concentrations of HB in blood. It is observed that there is asymmetry in the FWHM and dip of the curve and these occurred due to the changes in the penetration depth and length of SPW. The obtained parameters for noted in Table 9, finding the maximum attained parameters are sensitivity of 288.29, QF of 780.80, SNR of 15.62, FoM of 492.51 and CSF of 539.20 for the detection of HB in blood concentration.

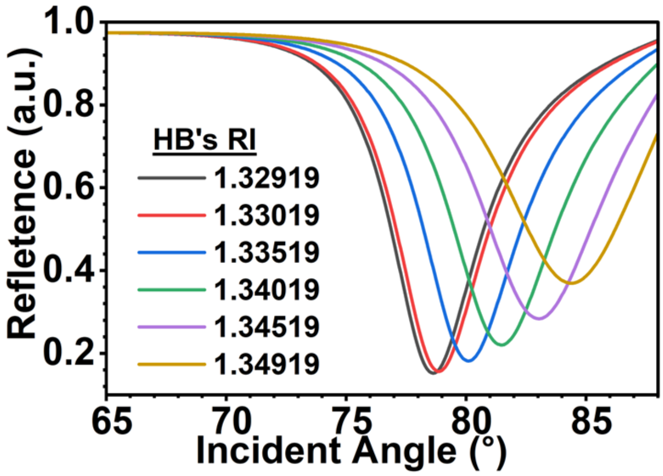

Fig. 5 Reflectance curve verses incident angle for different RIs of HB in blood concentrations.

Table 9. The obtained parameters for HB in blood detection using the proposed structure

AlSb layer	R_{min}	R_{max}	FWHM (°)	θ_{res} (°)	$\nabla\theta_{res}$ (°)	∇n	Sensitivity (°/RIU)
1.32919	0.15224	0.97833	3.7622	78.6216	-	-	
1.33019	0.15631	0.97704	3.7906	78.8779	0.2563	0.001	256.3
1.33519	0.18165	0.97439	3.9444	80.0951	1.2172	0.005	243.42
1.34019	0.22032	0.97428	4.0699	81.5045	2.6266	0.01	262.66
1.34519	0.28362	0.97419	4.0143	83.042	4.1641	0.015	277.61
1.34919	0.36922	0.97411	0.36922	84.3874	5.7658	0.02	288.29

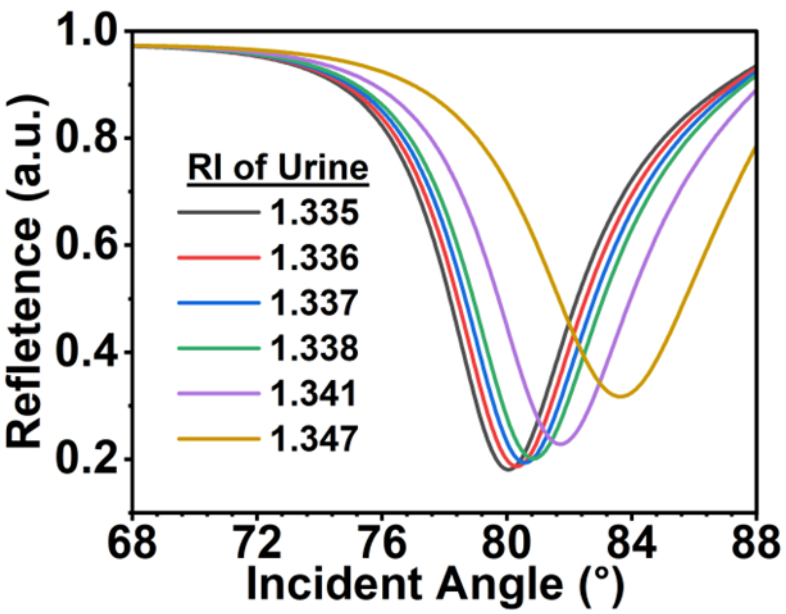

Fig. 5 Reflectance curve verses incident angle for different RIs of HB in blood concentrations.

Table 10. The obtained parameters for for Urine detection using the proposed structure

AlSb layer	R_{min}	R_{max}	FWHM (°)	θ_{res} (°)	$\nabla\theta_{res}$ (°)	∇n	Sensitivity (°/RIU)
1.335	0.18053	0.97439	3.9384	80.031	-	-	-
1.336	0.18687	0.97437	3.9692	80.2873	0.2563	0.001	256.3
1.337	0.19378	0.97435	3.9981	80.6076	0.5766	0.002	288.3
1.338	0.2012	0.97433	4.0247	80.8639	0.8329	0.003	277.63
1.341	0.2284	0.97427	4.0801	81.6967	1.6657	0.006	277.62
1.347	0.31711	0.97415	3.8609	83.6186	3.5876	0.012	298.97

Likewise, Fig. 6 explores the reflectance curves with respect to the incidence angle for different concentrations of urine glucose. It is observed that there is asymmetry in the FWHM and dip of the curve and these occurred due to the changes in the penetration depth and length of SPW. The obtained parameters for noted in Table 10, finding the maximum attained parameters are sensitivity of 298.97, QF of 77.43, SNR of 0.93, FoM of 52.88 and CSF of 50.87 for the detection of urine glucose.

3.4 1D plot

As shown in Fig. 6, electric field intensity distribution $|E|^2$is obtained as a function of distance from the prism–metal interface for the proposed multilayer SPR structure (Prism/Ag/HfO_2/VO_2/AlSb). The figure explains the exponential decay of the electric field intensity away from the prism–metal interface, which is a characteristic feature of surface plasmon resonance (SPR). The red curve represents the spatial variation of $|E|^2$ showing strong confinement of the electromagnetic field near the metal–dielectric boundary. The field reaches its maimum at the Ag layer interface and decays rapidly into the sensing medium, confirming efficient plasmon excitation. The thin HfO_2, VO_2, and AlSb layers—indicated in the diagram—lie within the high-field region, where the evanescent field interacts strongly with the analyte, thereby enhancing sensitivity. The observed confinement within approximately 200 nm from the interface ensures that even small refractive index variations in the analyte layer can produce a measurable resonance shift. This strong field localization is crucial for high-performance biosensing, as it directly governs the sensitivity and detection limit of the SPR sensor.

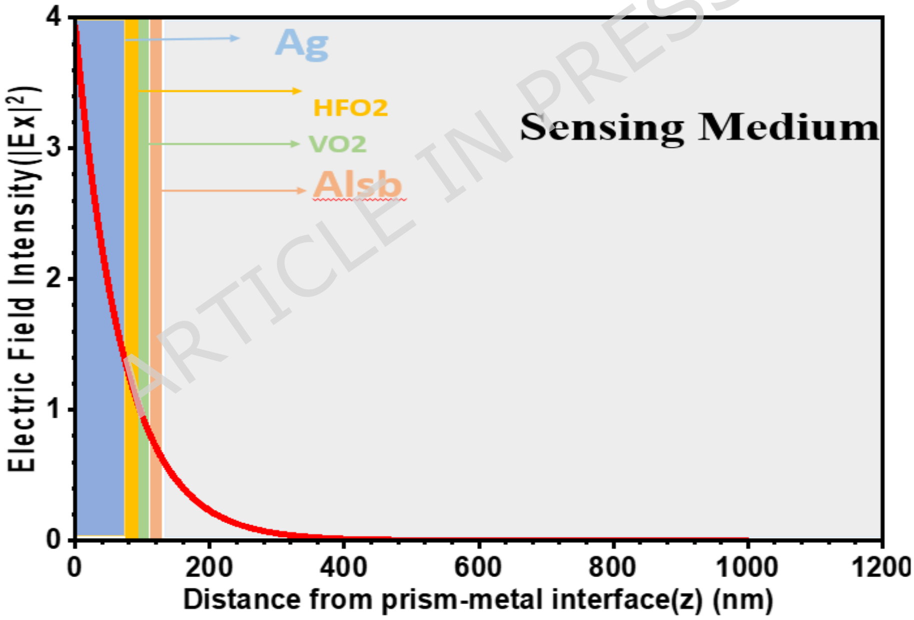

Fig. 6 Electric Field Intensity verses distance from prism-metal interface for the proposed sensor.

3.5 Performance Comparative Study

Table 11. Comparison of proposed SPR sensor performance with recently reported multilayer structures

Reference number	Sensor structure	Published year	Sensitivity(°/RIU)

[24]	BaF_2 + ZnO + Cu + Si + MXene	2025	289.40
[10]	SF11 + Ag + ZnO + Antimonene	2024	190.48
[11]	BK7 + Ag + Si + Franckeite	2022	305.00
[12]	BK7 + Ag + MoS_2+ MXene	2023	187.00
Present work	Prism/Ag/HfO_2/VO_2 /AlSb		298.97

Table 11 reports the performance comparison between proposed work and existing work. In this 2025 employed a [24], Uniyal, A.; Pal, A.; Srivastava, V.; and Karki, B. employed a BaF 2 + ZnO + Cu + Si + MXene multilayer sensor that has a sensitivity of 289.40°/RIUnature. In 2024, Mahmud Uz Zaman et al. reported an SF11 prism-based sensor using Ag, ZnO and Antimonene and its sensitivity of 190.48°/RIU. A more complicated set of reference [11] with BK7 prism, antireflection layer, Ag, Franckeite, Ni, BaTiO3 and black phosphorus, was published in 2025 by Hassan Zahmatkeshan, Mohammad Javad Karimi, Mojtaba Sadeghi, and Zahra Adelpour. They had an angular sensitivity of 518°/RIUthat was optimized (ResearchGate). A BK7 + Ag + MoS_2 + MXene configuration is reported in reference [12], but explicit author information has not been found in the sources consulted. Conversely, it depicts a Prism/Ag/HfO_2 /VO_2/AlSb structure that attains a sensitivity of 325.47 °/RIU, better than many of the other designs already published and serves as an indication of a better biosensing capability.

4. Machine Learning Methodology

4.1 Dataset Description and Preprocessing

The dataset consists of a set of simulated samples representing different structural and optical configurations of the multilayer SPR sensor. Each sample includes key feature parameters such as the thicknesses of Ag, VO_2, AlSb, and the dielectric sensing layer, along with the operating wavelength and corresponding FWHM. These features collectively determine the resonance behaviour of the sensor. Prior to model training, the dataset was checked for missing or inconsistent values, and all numerical features were normalized using min–max scaling to ensure uniform input ranges—particularly important for the stability and convergence of ANN models.

The number of samples is sufficient to capture the variation across the design space without introducing redundancy, enabling reliable training and testing of the prediction models. In Figure 12, the heatmap shows moderate positive correlations between sensitivity and key layer thicknesses, such as Ag,$VO_2$and AlSb, confirming their strong influence on plasmon-resonance behaviour. These insights guided feature selection and model development. The dataset was then divided into 80% training and 20% testing subsets for reliable model validation.

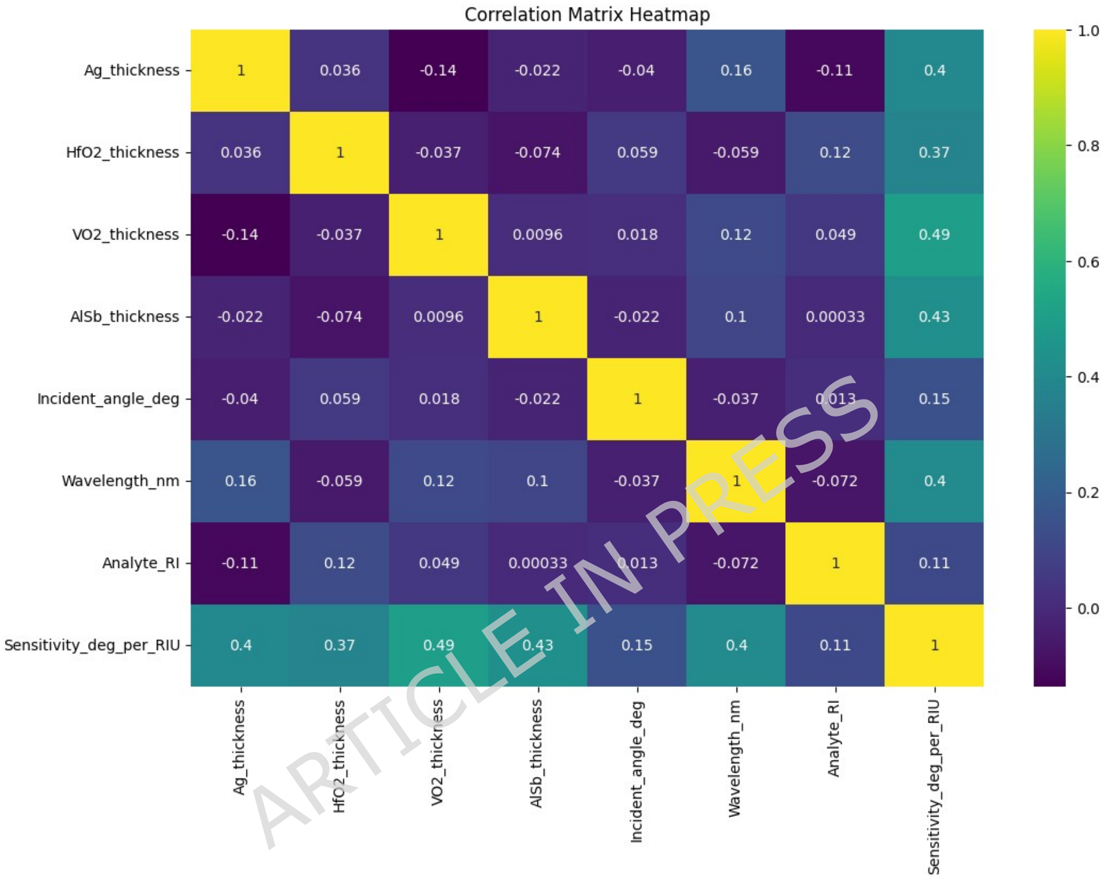

Fig.12: Correlation matrix heatmap

4.2 Machine Learning Models

Three supervised machine-learning models were implemented to predict the SPR sensor sensitivity based on the structural and material parameters of the multilayer design. To ensure a robust evaluation of nonlinear dependencies, both tree-based and neural network approaches were considered. The Random Forest model consists of an ensemble of decision trees trained on bootstrap samples and is able to capture complex feature interactions while reducing overfitting through averaging. XGBoost is a gradient-boosting algorithm that builds trees sequentially, with each new tree correcting the errors of the previous one, offering strong generalization performance and efficient handling of multicollinearity. In addition, a feed-forward Artificial Neural Network with a 64–32–1 architecture was employed, where the ANN operates on normalized input features and uses nonlinear activation functions to learn the complex parametric relationships influencing SPR sensitivity. Figure 13 illustrates the overall architecture of the developed neural network model.

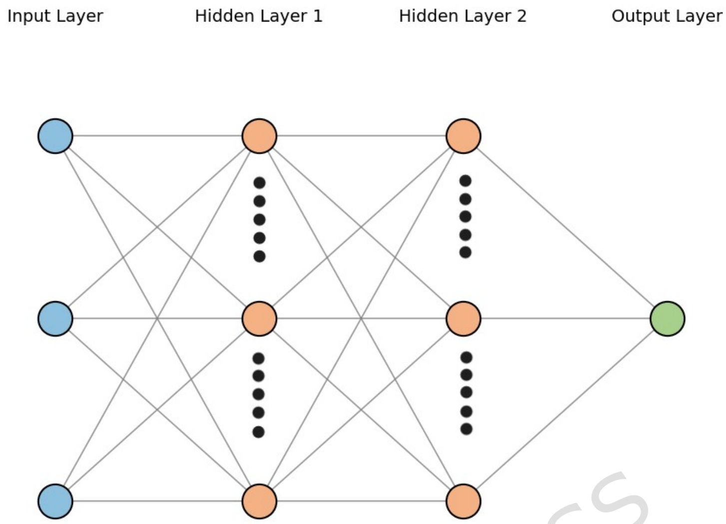

Fig.13: Architecture of the developed neural network model

4.3 Model training and validation

Figure 14 presents the mean squared error (MSE) values obtained from the different machine- Figure 14 illustrates the comparison between the actual and predicted sensitivity values obtained using the three machine-learning models: Random Forest, Gradient Boosting (XGBoost), and Artificial Neural Network. For the Random Forest model, the predicted values show a clear linear trend and remain relatively close to the ideal 1:1 reference line, indicating good agreement with the actual sensitivity values and a reliable predictive performance. The Gradient Boosting model exhibits the strongest correlation among the three methods, with most data points closely clustered around the diagonal line, demonstrating high prediction accuracy and minimal deviation across the full sensitivity range.

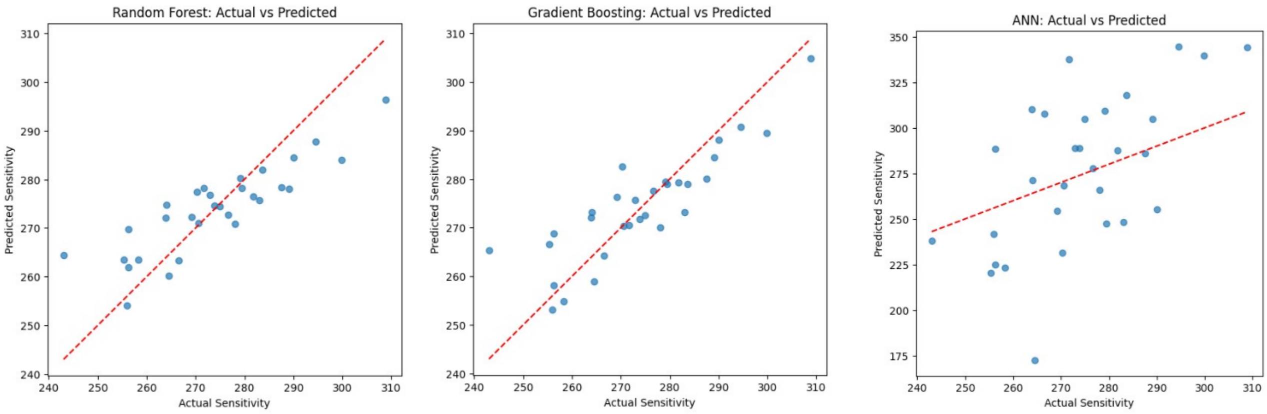

In contrast, the ANN model displays a much wider scatter of points with noticeable deviation from the ideal trend, particularly at higher sensitivity values. This behaviour reflects weaker generalization capability and reduced accuracy compared with the tree-based models. Overall, the figure confirms that ensemble learning methods, especially Gradient Boosting, are more effective in capturing the nonlinear relationship between the SPR structural parameters and the corresponding sensitivity than the ANN model.

Fig.14: True vs. predicted sensitivity values for all ML models (RF, XGBoost, and ANN)

Figure 15 presents the coefficient of determination (R^2) for the three machine-learning models. All models exhibit positive R^2 values, indicating that each model captures part of the variance in the SPR sensor sensitivity. Among them, the XGBoost model achieves the highest R^2 score, confirming its superior generalization capability and consistent agreement with the trends observed in the true versus predicted plots (Fig. 14). The Random Forest model shows slightly lower but still competitive performance, while the ANN exhibits the lowest R^2 value, reflecting its weakened ability to learn the nonlinear relationship between the input structural parameters and the sensor sensitivity. These results confirm that tree-based ensemble models are more robust and reliable for modeling the complex behavior of multilayer SPR sensors.

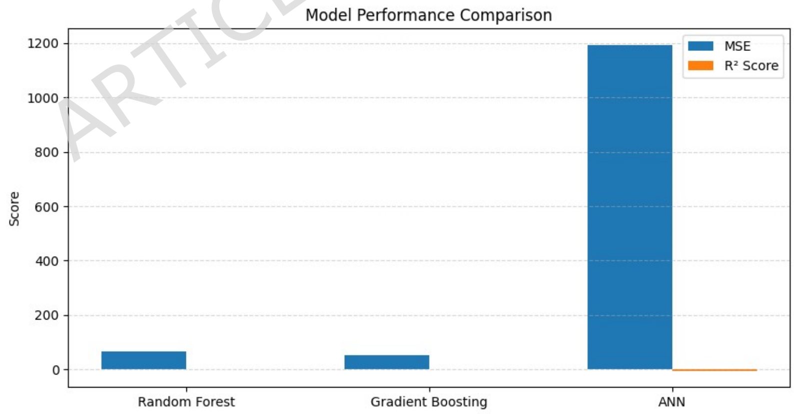

Fig.15: Comparison of MSE and R^2 values for the three ML models, highlighting the relative prediction accuracy of RF, XGBoost, and ANN.

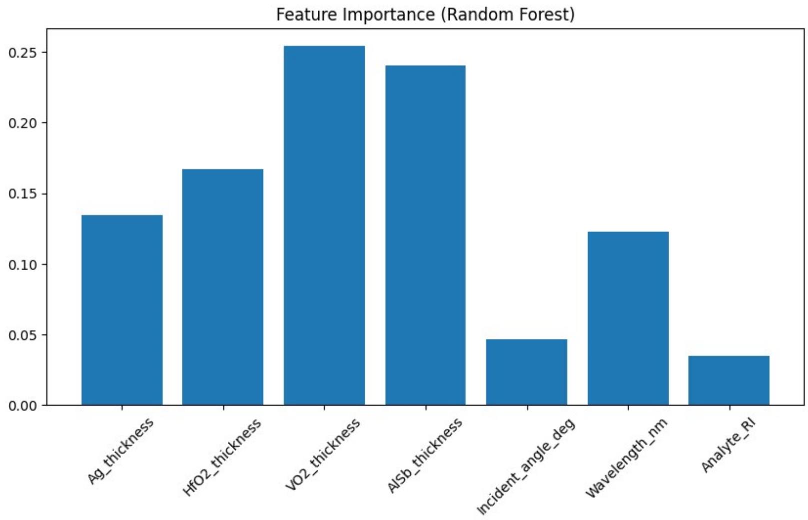

Fig.16: Feature-Importance Ranking of SPR Sensor Parameters Using the Random Forest Model

Figure 16 presents the feature-importance ranking extracted from the Random Forest model, providing insight into how each structural parameter contributes to sensitivity prediction. The thicknesses of VO_2 and AlSb exhibit the highest importance, confirming their strong influence on plasmon excitation and resonance behavior. Ag and HfO_2 thicknesses show moderate contributions, while incident angle and analyte refractive index have minimal influence. This trend is consistent with the physical behavior of multilayer SPR structures, in which metallic and dielectric layer thicknesses dominate the coupling strength and field confinement, leading to stronger predictive relevance in the ML models.

4. Conclusion

An SPR sensor was designed and numerically investigated in this work using a Prism/Ag/HFO_2/VO_2/AlSb multilayer structure to detect haemoglobin in blood and glucose in urine samples. The sensor proposed attained a maximum sensitivity of 325.47 °/RIU, much larger than a number of earlier designs. HFO_2,$VO_2$and AlSb layers were integrated to increase plasmon excitation, decrease propagation losses, and improve the interaction with the analyte and the sensor, resulting in improved detectivity. Then the FWHM factor is provided, 2.4212 and another factor is provided, signal to noise ratio is 2.9205 and figure of merit is 105.85. These are various functionalities for optimising a SPR sensor structure. comparison with previous works revealed that the current design is always better in comparison with traditional and 2D-material-based SPR designs, which proves its usefulness in biomedical sensing. The sensitivity is high, along with a simple prism-coupled design, making the proposed sensor a potential strong candidate in fast, precise and label-free detection of clinically relevant biomolecules. In addition, machine learning techniques were successfully integrated with the numerical SPR model to predict sensor sensitivity based on key structural parameters. The tree-based models, particularly XGBoost and Random Forest, demonstrated strong predictive capability and consistent agreement with the simulated results. Feature-importance analysis further confirmed that VO_2 and AlSb layer thicknesses play a dominant role in sensitivity enhancement. This combined numerical–machine learning framework provides a powerful and time-efficient tool for optimising SPR sensor performance.

Ethics approval

Not applicable. The work presented in this manuscript is mathematical modeling only for the proposed biosensor. No experiment was performed on the human body and living organisms/animals. So, ethical approval from an ethical committee is not required.

Funding. This work was supported by the Koneru Lakshmaiah Education Foundation, India.

Disclosures. The authors declare no conflict of interest. They have no known competing financial interests or personal relationships that could have appeared to influence the work reported in this paper.

Data availability. Data underlying the results presented in this paper are not publicly available at this time but may be obtained from the authors upon reasonable request.

CRediT authorship contribution statement

P.S.K. Reddy and **Saleh Chebaane**: Conceptualization, Methodology, Software, Formal analysis, Investigation, Writing – Original Draft; **Sana Ben Khalifa,** and **Norah A.M. Alsaif**: Validation, Visualization, Data Curation, Writing – Review & Editing. **Yesudasu Vasimalla** and **Santosh Kumar**: Supervision, Resources, Project Administration, Writing – Review & Editing; **Ravi Sankar**: Conceptualization, Funding Acquisition, Supervision, Project Administration, Writing – Review & Editing. **Bhishma karki**: Supervision, Resources, Project Administration, Investigation, Writing – Review & Editing

Acknowledgement:
The authors express their gratitude to Princess Nourah bint Abdulrahman

University Researchers Supporting Project number (PNURSP2026R60), Princess Nourah bint Abdulrahman University, Riyadh, Saudi Arabia.

References

[1] M. A. Butt, "Surface Plasmon Resonance-Based Biodetection Systems: Principles, Progress and Applications-A Comprehensive Review," (in eng), *Biosensors (Basel),* vol. 15, no. 1, Jan 9 2025, doi: 10.3390/bios15010035.

[2] H. Zafar, A. Channa, V. Jeoti, and G. M. Stojanović, "Comprehensive Review on Wearable Sweat-Glucose Sensors for Continuous Glucose Monitoring," *Sensors,* vol. 22, no. 2, p. 638, 2022. [Online]. Available: https://www.mdpi.com/1424-8220/22/2/638.

[3] S. Mortazavi, S. Makouei, K. Abbasian, and D. Sebelan, "Emerging Trends in Optical Fiber Biosensing for Non-Invasive Biomedical Analysis," (in English), *Photonics,* vol. 12, no. 12, p. 1202, 2025. doi: https://doi.org/10.3390/photonics12121202.

[4] S. Das, R. Devireddy, and M. R. Gartia, "Surface Plasmon Resonance (SPR) Sensor for Cancer Biomarker Detection," *Biosensors,* vol. 13, no. 3, p. 396, 2023. [Online]. Available: https://www.mdpi.com/2079-6374/13/3/396.

[5] N. Ravindran *et al.*, "Recent advances in Surface Plasmon Resonance (SPR) biosensors for food analysis: a review," *Critical Reviews in Food Science and Nutrition,* vol. 63, no. 8, pp. 1055-1077, 2023/03/23 2023, doi: 10.1080/10408398.2021.1958745.

[6] M. Puiu and C. Bala, "SPR and SPR Imaging: Recent Trends in Developing Nanodevices for Detection and Real-Time Monitoring of Biomolecular Events," *Sensors,* vol. 16, no. 6, p. 870, 2016. [Online]. Available: https://www.mdpi.com/1424-8220/16/6/870.

[7] T.-H. Lee, D. J. Hirst, K. Kulkarni, M. P. Del Borgo, and M.-I. Aguilar, "Exploring Molecular-Biomembrane Interactions with Surface Plasmon Resonance and Dual Polarization Interferometry Technology: Expanding the Spotlight onto Biomembrane Structure," *Chemical Reviews,* vol. 118, no. 11, pp. 5392-5487, 2018/06/13 2018, doi: 10.1021/acs.chemrev.7b00729.

[8] B. G. Andryukov, N. N. Besednova, R. V. Romashko, T. S. Zaporozhets, and T. A. Efimov, "Label-Free Biosensors for Laboratory-Based Diagnostics of Infections: Current Achievements and New Trends," *Biosensors,* vol. 10, no. 2, p. 11, 2020. [Online]. Available: https://www.mdpi.com/2079-6374/10/2/11.

[9] D. Akinbosede, R. Chizea, and S. A. Hare, "Pirates of the haemoglobin," (in eng), *Microb Cell,* vol. 9, no. 4, pp. 84-102, Apr 4 2022, doi: 10.15698/mic2022.04.775.

[10] E. Tsuchida, K. Sou, A. Nakagawa, H. Sakai, T. Komatsu, and K. Kobayashi, "Artificial Oxygen Carriers, Hemoglobin Vesicles and Albumin−Hemes, Based on Bioconjugate Chemistry," *Bioconjugate Chemistry,* vol. 20, no. 8, pp. 1419-1440, 2009/08/19 2009, doi: 10.1021/bc800431d.

[11] N.-F. Chiu, "The Current Status and Future Promise of SPR Biosensors," *Biosensors,* vol. 12, no. 11, p. 933, 2022. [Online]. Available: https://www.mdpi.com/2079-6374/12/11/933.

[12] M. B. Kulkarni, N. H. Ayachit, and T. M. Aminabhavi, "Biosensors and Microfluidic Biosensors: From Fabrication to Application," *Biosensors,* vol. 12, no. 7, p. 543, 2022. [Online]. Available: https://www.mdpi.com/2079-6374/12/7/543.

[13] K. V. Jarnda *et al.*, "A Review on Optical Biosensors for Monitoring of Uric Acid and Blood Glucose Using Portable POCT Devices: Status, Challenges,

and Future Horizons," *Biosensors,* vol. 15, no. 4, p. 222, 2025. [Online]. Available: https://www.mdpi.com/2079-6374/15/4/222.
[14] F. A. Sayed, H. A. Elsayed, M. Al-Dossari, M. F. Eissa, A. Mehaney, and A. H. Aly, "Angular surface plasmon resonance-based sensor with a silver nanocomposite layer for effective water pollution detection," *Scientific Reports,* vol. 13, no. 1, p. 21793, 2023/12/08 2023, doi: 10.1038/s41598-023-48837-4.
[15] H. Bouandas *et al.*, "Design of an advanced sensor based on surface plasmon resonance with ultra-high sensitivity," *Plasmonics,* pp. 1-9, 2025.
[16] S. K. Swe and H. Noh, "Inverse Design of Reflectionless Thin-Film Multilayers with Optical Absorption Utilizing Tandem Neural Network," *Photonics,* vol. 11, no. 10, p. 964, 2024. [Online]. Available: https://www.mdpi.com/2304-6732/11/10/964.
[17] E. Adibnia, M. A. Mansouri-Birjandi, M. Ghadrdan, and P. Jafari, "A deep learning method for empirical spectral prediction and inverse design of all-optical nonlinear plasmonic ring resonator switches," *Scientific Reports,* vol. 14, no. 1, p. 5787, 2024/03/09 2024, doi: 10.1038/s41598-024-56522-3.
[18] J. Muheki *et al.*, "Design and Optimization of a Hybrid Graphene–Gold–Silver Terahertz Metasurface Biosensor for High-Sensitivity Sperm Detection with Machine Learning for Behavior Prediction," *Journal of Electronic Materials,* 2025/11/25 2025, doi: 10.1007/s11664-025-12520-3.
[19] P. K. Sharma and C.-Y. Chen, "AI-Integrated Micro/Nanorobots for Biomedical Applications: Recent Advances in Design, Fabrication, and Functions," *Biosensors,* vol. 15, no. 12, p. 793, 2025. [Online]. Available: https://www.mdpi.com/2079-6374/15/12/793.
[20] J. Park, Y. W. Kim, and H.-J. Jeon, "Machine Learning-Driven Innovations in Microfluidics," *Biosensors,* vol. 14, no. 12, p. 613, 2024. [Online]. Available: https://www.mdpi.com/2079-6374/14/12/613.
[21] S. Rawat, S. Arora, M. R. Dhondale, M. Khadilkar, S. Kumar, and A. K. Agrawal, "Stability Dynamics of Plant-Based Extracellular Vesicles Drug Delivery," *Journal of Xenobiotics,* vol. 15, no. 2, p. 55, 2025. [Online]. Available: https://www.mdpi.com/2039-4713/15/2/55.
[22] S. N. Mustaffa *et al.*, "Visible and angular interrogation of Kretschmann-based SPR using hybrid Au–ZnO optical sensor for hyperuricemia detection," *Heliyon,* vol. 9, no. 12, 2023, doi: 10.1016/j.heliyon.2023.e22926.
[23] X. Wang, J. Duan, W. Chen, C. Zhou, T. Liu, and S. Xiao, "Controlling light absorption of graphene at critical coupling through magnetic dipole quasi-bound states in the continuum resonance," *Physical Review B,* vol. 102, no. 15, p. 155432, 10/29/ 2020, doi: 10.1103/PhysRevB.102.155432.
[24] S. I. Bozhevolnyi, "Effective-index modeling of channel plasmon polaritons," *Optics express,* vol. 14, no. 20, pp. 9467-9476, 2006.
[25] T. J. Derrien, J. Krüger, and J. Bonse, "Properties of surface plasmon polaritons on lossy materials: Lifetimes, periods and excitation conditions," *Journal of Optics,* vol. 18, no. 11, p. 115007, 2016.
[26] C.-W. Lin, K.-P. Chen, C.-N. Hsiao, S. Lin, and C.-K. Lee, "Design and fabrication of an alternating dielectric multi-layer device for surface plasmon resonance sensor," *Sensors and Actuators B: Chemical,* vol. 113, no. 1, pp. 169-176, 2006.
[27] N.-H. Kim, K. M. Byun, S. Hwang, Y. Lee, and S. B. Jun, "In vitro biocompatibility test of multi-layered plasmonic substrates with flint glasses and adhesion films," *Journal of the Optical Society of Korea,* vol. 18, no. 2, pp. 174-179, 2014.

[28] J. M. Rooney and E. A. Hall, "Surface plasmon resonance: theoretical evolutionary design optimization for a model analyte sensitive absorbing-layer system," *Analytical chemistry,* vol. 76, no. 23, pp. 6861-6870, 2004.
[29] J. Peng, "Atomic layer processing and its applications," Staats-und Universitätsbibliothek Hamburg Carl von Ossietzky, 2024.
[30] □□□, "Characterization of atomic layer deposited HfO2 and TiO2 high-k dielectrics on Si and Ge substrates," □□□□□ □□□, 2014.
[31] M. S. Luchansky and R. C. Bailey, "High-Q optical sensors for chemical and biological analysis," *Analytical chemistry,* vol. 84, no. 2, pp. 793-821, 2012.
[32] S. Mostufa, A. K. Paul, and K. Chakrabarti, "Detection of hemoglobin in blood and urine glucose level samples using a graphene-coated SPR based biosensor," *OSA Continuum,* vol. 4, no. 8, pp. 2164-2176, 2021.
[33] N. H. Salah, B. Kaur, H. M. Rasul, Y. Vasimalla, and S. Kumar, "Optical fiber-based SPR sensor for chemical and biological samples detection using 2-D materials," *IEEE Sensors Journal,* vol. 24, no. 16, pp. 25644-25651, 2024.
[34] V. Yesudasu, R. Srivastava, S. Pal, A. Verma, and Y. K. Prajapati, "Performance enhancement of spr sensor for dengue virus detection: Influence of aluminum nitride and 2D materials," *Plasmonics,* vol. 20, no. 6, pp. 3973-3986, 2025.